Impact of GNSS output frequency and antenna position on vehicle modeling in motorcycle localization

Stefano Radrizzani, Giorgio Riva and Giulio Panzani

***Abstract*— Autonomous driving for motorcycles has received comparatively little attention, despite the extensive research on four-wheeled vehicles. Motorcycles pose unique challenges due to their inherently wide ranges of roll and pitch dynamics, which can significantly influence accurate vehicle localization. In this work, we investigate the necessity of incorporating roll and pitch angles in motorcycle localization models, analyzing how Global Navigation Satellite System (GNSS) output frequency and antenna position influence their performance within Kalman-filter based algorithms. First, we present a formal analysis of the impact of roll and pitch angles on both model integration and output computation as a function of GNSS output frequency and antenna location. Then, we provide a quantitative evaluation using real experimental data to validate the theoretical findings, spanning the GNSS frequency from a low-cost commercial sensor to an ideal one. The results provide both methodological and practical insights into vehicle modeling for Kalman-filter localization of two-wheeled tilting vehicles.**

I. Introduction

Autonomous Driving (AD) represents one of the most significant challenges in the automotive sector [1]. While AD for four-wheeled vehicles is extensively studied in the literature, two-wheeled vehicles, i.e., motorcycles, have received comparatively little attention. Existing research on motorcycles is mainly focused on stabilization control, due to their intrinsic dynamic instability, see for example [2]. As discussed in [3], a complete AD stack typically relies on a modular architecture in which perception, planning, control, and localization cooperate to accomplish the navigation task. Specifically, for the localization problem, the objective is to estimate the vehicle position with respect to a fixed reference frame with high accuracy, ensuring that the planning and control modules can operate safely and reliably. As summarized in [4], numerous localization algorithms and techniques have been developed for four-wheeled vehicles on different sensor suites and for different, as urban or racing, applications (see respectively [5] and [6] for recent advances in these domains). In this context, Inertial Navigation Systems (INS), which rely solely on accelerations and angular rates measurements, suffer from drift errors, whereas centimeter-accuracy absolute sensors, such as double antenna Global Navigation Satellite System (GNSS) with Real Time Kinematics (RTK) correction, typically operate at limited output frequencies. As a consequence, INS-GNSS sensor fusion has become the most established technique to achieve accurate and high-rate localization. A wide variety of Kalman-filter (KF) based estimation techniques have been proposed in the literature, see e.g., [7] and [8], most of which employ a planar kinematic model of the vehicle (see [9]), since roll and pitch angles are typically negligible in four-wheeled vehicles.

Regarding motorcycles, instead, very few works address the localization problem. [10] proposes to identify motorcycles positions in road environments using external cameras, whereas [11] and [12] discuss more classical KF-based approaches built on three-dimensional kinematic models that explicitly account for roll and pitch dynamics. The need of roll and pitch angles is motivated by the fact that their ranges are typically much wider than in four-wheeled vehicles, thus potentially increasing localization accuracy, since the performance of any model-based algorithm is inherently tied to the fidelity of the underlying model. At the same time, however, these approaches require precise estimation of roll and pitch angles. Moreover, the output frequency of the employed GNSS also plays an important role, as it determines how long the localization module must rely on the vehicle model before a new absolute high-accuracy information becomes available, which may impose different requirements on the complexity of the vehicle model. Hence, in this work, we aim to investigate the necessity of including roll and pitch angles in the localization model as a function of both the positioning of the GNSS antenna on the vehicle and its output frequency, spanning from a low-cost commercial sensor to an ideal sensor sampling at the ECU frequency. This analysis provides both methodological and practical insights into localization for two-wheeled vehicles. Specifically, the contributions of this paper are twofold: (i) a formal analysis of the impact of including roll and pitch angles, considering GNSS output frequency and antenna position, on both the model integration and output computation, with the latter evaluated against GNSS measurements in a KF-based algorithm; (ii) a quantitative analysis based on real experimental data to show the consistency of the mathematical findings in a real world scenario.

In the remainder of the paper, Section II describes the experimental setup and the dataset. Section III and IV present and validate a formal analysis of the impact of roll and

The authors are with Dipartimento di Elettronica, Informazione e Bioingegneria, Politecnico di Milano, Via G. Ponzio 34/5, 20133, Milan, Italy. Corresponding author: Stefano Radrizzani stefano.radrizzani@polimi.it.

This study has been partially supported by MOST - Sustainable Mobility National Research Center and received funding from the European Union Next-GenerationEU (PIANO NAZIONALE DI RIPRESA E RESILIENZA (PNRR) - MISSIONE 4 COMPONENTE 2, INVESTIMENTO 1.4 - D.D. 1033 17/06/2022, CN00000023). This manuscript reflects only the authors' views and opinions, neither the European Union nor the European Commission can be considered responsible for them. This paper has been partially supported from Italian Ministerial grant PRIN 2022 "AGeNT" ID 20223F5SZB.

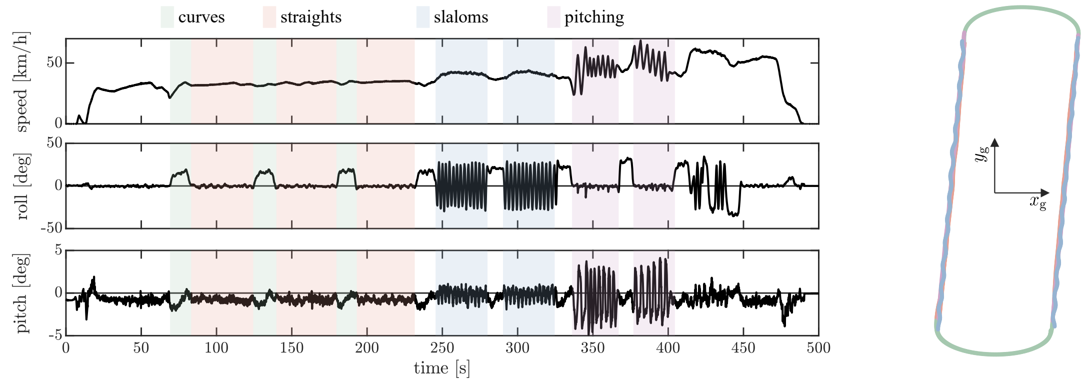

Fig. 1. **Dataset collected at CREA oval-like proving-ground in Treviglio, Italy**. The time evolution of speed, roll and pitch angles is shown on the left, while GNSS traces are shown on the right. For analysis purposes, the dataset is divided into four categories: straights, corners, slaloms, and pitching zones.

pitch angles in the vehicle model for localization. Section V concludes the paper with remarks.

II. Experimental Setup and Dataset Description

The motorcycle used in this work, previously presented in [13], is an *Eva Ribelle*, i.e., a commercial electric motorcycle manufactured by Energica Motor Company (Modena, Italy). The vehicle has been retrofitted at Politecnico di Milano (Milan, Italy) with all actuators, sensors, and control units required to enable up to full autonomous riding. In this section, we describe the sensors relevant for localization, as illustrated in Fig. 2. An **Optical Sensor Unit (OSU)**, a non-contact speed sensor is mounted on the underside of the motorcycle to measure the longitudinal and lateral velocities and also provide estimates of the roll and pitch angles; a **6-axis Inertial Measurement Unit (IMU)** measures the chassis linear accelerations and the angular velocities; a **Global Navigation Satellite System (GNSS)** is available with a multi-constellation receiver with Real Time Kinematic (RTK) capability with front and rear antennas. An **Electronic Control Unit (ECU)** is employed as data-logger and real-time controller to execute the main algorithm, responsible for vehicle dynamics control, state estimation and localization, at a sampling frequency of 100 Hz.

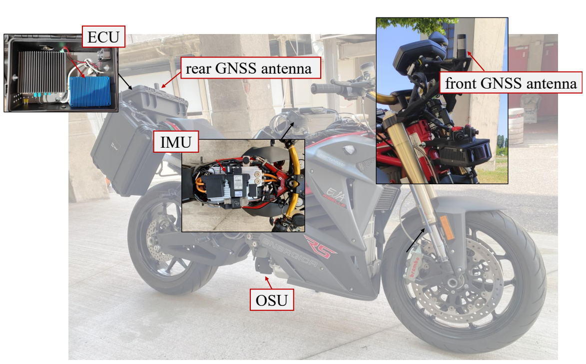

Fig. 2. **Experimental setup**: a retrofitted Energica *Eva Ribelle*, equipped with an Optical Sensor Unit for speed and roll/pitch estimation, a 6-axis IMU, two GNSS antennas and a Speedgoat ECU.

The experimental data used in this paper were collected at the CREA proving ground in Treviglio, Italy, an oval-like test-track where a variety of standard maneuvers were executed. The whole dataset, illustrated in Fig. 1, has been categorized into four classes of maneuvers: **straights**, straight-lines driven at constant speed without roll motion; **curves**, curved-segments driven at constant speed and approximately constant roll angle; **slaloms**, straight-line segments driven at constant speed with varying roll angle; **pitching**, straight-line segments driven with alternating acceleration and braking to induce pitch dynamics.

We highlight that, to evaluate the performance of the localization model and to analyze the impact of the antenna position and of different GNSS output frequencies in Section IV, an ideal position benchmark was reconstructed offline using the rear antenna measurements. Specifically: (i) GNSS data, originally sampled at 10 Hz, have been resampled at 100 Hz, to match the ECU execution rate; and (ii) sampling delays were compensated using the GNSS-provided timestamps of each navigation epoch. This can be done because GNSS and the ECU are synchronized via PTP (Precision Time Protocol).

III. Vehicle Models for Localization: Formulation and Analysis

In this section, we discuss the kinematic vehicle models employed within a KF-based motorcycle localization framework, progressively transitioning from a complete three-dimensional motorcycle model to simplified, car-like formulations in which roll and pitch dynamics are neglected. We first introduce the mathematical formulations of the considered models along with their underlying assumptions. Then, we formally analyze the impact that roll and pitch angles have on both model integration and output measurement, highlighting how these effects depend on the GNSS output frequency and on the position of the antenna on the vehicle. To ease the notation, we adopt the following shorthand for trigonometric functions: $\mathrm{c}_x = \cos(x)$, $\mathrm{s}_x = \sin(x)$, $\mathrm{t}_x = \tan(x)$.

TABLE I

LOCALIZATION MODELS.

	motorcycle $\mathscr{M}(\varphi,\vartheta,v_{\text{vf}},\omega_{\text{vf}})$	**no-pitch** $\Phi(\varphi,v_{\text{vf}},\omega_{\text{vf}})$	**no-roll** $\Theta(\vartheta,v_{\text{vf}},\omega_{\text{vf}})$	**car** $\mathscr{C}(v_{\text{vf}},\omega_{\text{vf}})$
$\dot{\hat{p}} =$	$E\cdot R(\varphi,\vartheta,\hat{\psi})v_{\text{vf}}$	$E\cdot R_z(\hat{\psi})R_x(\varphi)v_{\text{vf}}$	$E\cdot R_z(\hat{\psi})R_y(\vartheta)v_{\text{vf}}$	$E\cdot R_z(\hat{\psi})v_{\text{vf}}$
$\dot{\hat{\psi}} =$	$\omega_y\frac{\mathrm{s}_\varphi}{\mathrm{c}_\vartheta}+\omega_z\frac{\mathrm{c}_\varphi}{\mathrm{c}_\vartheta}$	$\omega_y\mathrm{s}_\varphi+\omega_z\mathrm{c}_\varphi$	$\omega_z\frac{1}{\mathrm{c}_\vartheta}$	ω_z
$\hat{p}_{\text{g}} =$	$\hat{p}+E\cdot R(\varphi,\vartheta,\hat{\psi})d_{\text{g}}$	$\hat{p}+E\cdot R_z(\hat{\psi})R_x(\varphi)d_{\text{g}}$	$\hat{p}+E\cdot R_z(\hat{\psi})R_y(\vartheta)d_{\text{g}}$	$\hat{p}+E\cdot R_z(\hat{\psi})d_{\text{g}}$

A. Kinematic Models: Formulation

We begin by introducing the full motorcycle kinematic model, illustrated in Fig. 3. As a three-dimensional rigid body, the motorcycle orientation in space is described using Euler angles, following the roll–pitch–yaw convention. Specifically, roll, pitch, and yaw angles are denoted by φ, ϑ, and ψ, respectively. As shown in Fig. 3, three reference frames are defined: (i) the global reference frame (gf), which is inertial; (ii) the road reference frame (rf), which shares the same yaw angle ψ as the vehicle; and (iii) the vehicle reference frame (vf), which is rigidly attached to the motorcycle. A vector w expressed in the vehicle frame, denoted w_{vf}, can be mapped into the road and global frames as

$$\begin{aligned} w_{\text{rf}} &= R_y(\vartheta)R_x(\varphi)w_{\text{vf}} \\ w_{\text{gf}} &= R(\varphi,\vartheta,\psi)w_{\text{vf}} = R_z(\psi)R_y(\vartheta)R_x(\varphi)w_{\text{vf}}, \end{aligned} \tag{1}$$

where $R_x(\varphi)$, $R_y(\vartheta)$, and $R_z(\psi)$ are the elementary rotation matrices (see [14] for details). Moreover, the time derivatives of the Euler angles are related to the angular velocity of the body $\omega_{\text{vf}} = [\omega_x\ \omega_y\ \omega_z]'$ through

$$\begin{cases} \dot{\varphi} = \omega_x + \omega_y \mathrm{t}_\vartheta \mathrm{s}_\varphi + \omega_z \mathrm{t}_\vartheta \mathrm{c}_\varphi \\ \dot{\vartheta} = \omega_y \mathrm{c}_\varphi - \omega_z \mathrm{s}_\varphi \\ \dot{\psi} = \omega_y \dfrac{\mathrm{s}_\varphi}{\mathrm{c}_\vartheta} + \omega_z \dfrac{\mathrm{c}_\varphi}{\mathrm{c}_\vartheta}. \end{cases} \tag{2}$$

Given that our objective is the vehicle localization, we focus exclusively on the position of the motorcycle in the ground plane and on its ψ orientation. Accordingly, the localization model $\mathscr{M}$, which governs the time evolution of the vehicle position and yaw angle, is defined as

$$\mathscr{M}(\varphi,\vartheta,v_{\text{vf}},\omega_{\text{vf}}) : \begin{cases} \dot{\hat{p}} = E\cdot R(\varphi,\vartheta,\hat{\psi})v_{\text{vf}} \\ \dot{\hat{\psi}} = \omega_y \dfrac{\mathrm{s}_\varphi}{\mathrm{c}_\vartheta} + \omega_z \dfrac{\mathrm{c}_\varphi}{\mathrm{c}_\vartheta} \\ \hat{p}_{\text{g}} = \hat{p} + E\cdot R(\varphi,\vartheta,\hat{\psi})d_{\text{g}} \end{cases} \tag{3}$$

where $\hat{p} = \begin{bmatrix}\hat{x}\ \hat{y}\end{bmatrix}'$ and $\hat{p}_{\text{g}} = \begin{bmatrix}\hat{x}_{\text{g}}\ \hat{y}_{\text{g}}\end{bmatrix}'$ denote, respectively, the estimated ground-projected position of the center of gravity (CoG) and the estimated global frame position of the rear GNSS antenna. The input velocity $v_{\text{vf}} = \begin{bmatrix}v_x\ v_y\ 0\end{bmatrix}'$ is defined at the ground projection of the CoG expressed in the vehicle reference frame. The vector $d_{\text{g}} = \begin{bmatrix}d_x\ d_y\ d_z\end{bmatrix}'$ is a constant vector in the vehicle frame which represents the mounting distance between the ground-projected CoG position and the GNSS antenna. Finally, the matrix

$$E = \begin{bmatrix}1 & 0 & 0\\ 0 & 1 & 0\end{bmatrix} \tag{4}$$

extracts only the planar components of a three-dimensional vector, ensuring that only the x and y coordinates are considered.

Given that the aim of this paper is to analyze the role of the vehicle model within localization algorithms, three simplified models are introduced in Table I. The starting point is Model $\mathscr{M}$, defined in (3), which is referred to as the *motorcycle model*, since it incorporates both roll and pitch angles. The opposite model, $\mathscr{C}$, called *car model*, neglects these two angles, which are typically small in four-wheeled vehicles. Additionally, two intermediate models, Θ and Φ, referred to as the *no-roll* and *no-pitch* models, respectively, neglect the roll and the pitch angles individually.

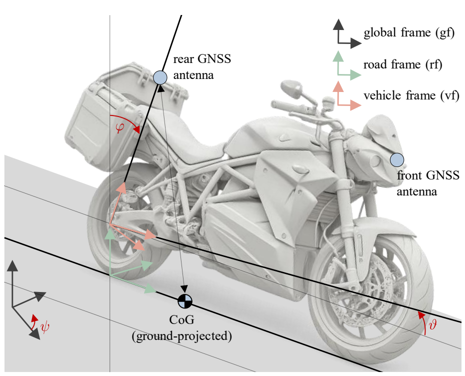

Fig. 3. **Motorcycle kinematic model**. The three reference frames used in the formulation are shown: (i) global reference frame (gf), (ii) road reference frame (rf), and (iii) vehicle reference frame (vf). The position of the two GNSS antennas and the ground-projected CoG on the experimental motorcycle are also indicated.

B. Kinematic Models: Roll and Pitch Impact Analysis

The analysis of the localization models aims to determine whether, and under which conditions, roll and pitch angles are relevant in motorcycle localization. Specifically, we focus on the application of the models introduced in Section III-A within KF-based algorithms. To this end, we formally analyze the impact of roll and pitch angles on two key aspects: (i) the *integration model*, by quantifying the drifts induced as a function of the output GNSS frequency, which defines the expected integration interval of the model $T_{\text{g}} = f_{\text{g}}^{-1}$, where f_{g} is the GNSS output frequency; and (ii) the *output equation*, which determines the error used by a KF to correct the model state variables. Indeed, errors in the output equation will reflect on wrong state estimates. In this formal analysis, we compare the motorcycle model against the car model. Specifically, the impact of roll and pitch angles is mathematically evaluated using three metrics. The first metric, referred to as *position integration mismatch*, is defined as the norm of the difference in linear velocity between the models, multiplied by the integration time T_{g}:

$$\begin{aligned}\|\Delta\hat{p}\| &= \|E\cdot R_z(\hat{\psi})v_{\mathrm{vf}} - E\cdot R(\varphi,\vartheta,\hat{\psi})v_{\mathrm{vf}}\|\,T_{\mathrm{g}} = \\ &= \left\|E\cdot R_z(\psi)\left[I - R_y(\vartheta)R_x(\varphi)\right]v_{\mathrm{vf}}\right\|T_{\mathrm{g}} = \\ &= \left\|E\cdot\left[I - R_y(\vartheta)R_x(\varphi)\right]v_{\mathrm{vf}}\right\|T_{\mathrm{g}} = \\ &= \|W(\varphi,\vartheta)v_{\mathrm{vf}}\|\,T_{\mathrm{g}},\end{aligned} \tag{5}$$

where $W(\varphi,\vartheta) = E\cdot[I - R_y(\vartheta)R_x(\varphi)]$. The second metric, named *heading integration mismatch*, is defined as the norm of the difference in yaw rate between the two models, multiplied by the integration time T_{g}:

$$|\Delta\hat{\psi}| = \left|-\omega_y\frac{\mathrm{s}_\varphi}{\mathrm{c}_\vartheta} + \omega_z\left(1 - \frac{\mathrm{c}_\varphi}{\mathrm{c}_\vartheta}\right)\right|T_{\mathrm{g}}. \tag{6}$$

Finally, the third metric, the *output position mismatch*, computes the norm of the difference between the two output equations of the two models:

$$\begin{aligned}\|\Delta\hat{p}_{\mathrm{g}}\| &= \left\|\hat{p} + E\cdot R_z(\hat{\psi})d_{\mathrm{g}} - \hat{p} - E\cdot R(\varphi,\vartheta,\hat{\psi})d_{\mathrm{g}}\right\| = \\ &= \left\|E\cdot R_z(\psi)\left[I - R_y(\vartheta)R_x(\varphi)\right]d_{\mathrm{g}}\right\| = \\ &= \left\|E\cdot\left[I - R_y(\vartheta)R_x(\varphi)\right]d_{\mathrm{g}}\right\| = \\ &= \left\|W(\varphi,\vartheta)d_{\mathrm{g}}\right\|.\end{aligned} \tag{7}$$

Therefore, it is evident from (5) and (7) that a crucial role in both the position integration and output mismatches is played by the matrix

$$W(\varphi,\vartheta) = E\cdot\left[I - R_y(\vartheta)R_x(\varphi)\right], \tag{8}$$

which acts as a weighting matrix for the speed v_{vf} in (5) or GNSS displacement vector d_{g} in (7). After straightforward matrix computations, $W(\varphi,\vartheta)$ can be expressed as

$$W(\varphi,\vartheta) = \begin{bmatrix} 1-\mathrm{c}_\vartheta & -\mathrm{s}_\vartheta\mathrm{s}_\varphi & -\mathrm{c}_\varphi\mathrm{s}_\vartheta \\ 0 & 1-\mathrm{c}_\varphi & \mathrm{s}_\varphi \end{bmatrix}. \tag{9}$$

Consequently, the two mismatches can be explicitly interpreted as functions of roll φ and pitch ϑ angles as

$$\|\Delta\hat{p}\| = \left\|\begin{bmatrix} v_x\left(1-\mathrm{c}_\vartheta\right) - v_y\mathrm{s}_\vartheta\mathrm{s}_\varphi \\ v_y\left(1-\mathrm{c}_\varphi\right)\end{bmatrix}\right\|T_{\mathrm{g}}, \tag{10}$$

and

$$\|\Delta\hat{p}_{\mathrm{g}}\| = \left\|\begin{bmatrix} d_x\left(1-\mathrm{c}_\vartheta\right) - d_z\mathrm{c}_\varphi\mathrm{s}_\vartheta \\ d_z\mathrm{s}_\varphi\end{bmatrix}\right\|, \tag{11}$$

where, for simplicity, we assume that the lateral displacement of the antenna $d_y \approx 0$ for any mounting position, due to the limited width of motorcycles. This assumption is consistent with the specific vehicle used in the experimental analysis. Since combined rolling and pitching is rare in standard motorcycle maneuvers, we can set either $\vartheta = 0$ or $\varphi = 0$ to facilitate the interpretation of the analysis. Under these assumptions, the mismatches become

	$\vartheta = 0$	$\varphi = 0$
$\|\Delta\hat{p}\|$	$\left\lvert v_y\left(1-\mathrm{c}_\varphi\right)\right\rvert T_{\mathrm{g}}$	$\left\lvert v_x\left(1-\mathrm{c}_\vartheta\right)\right\rvert T_{\mathrm{g}}$
$\lvert\Delta\hat{\psi}\rvert$	$\left\lvert -\omega_y\mathrm{s}_\varphi + \omega_z\left(1-\mathrm{c}_\varphi\right)\right\rvert T_{\mathrm{g}}$	$\left\lvert \omega_z\left(1-\frac{1}{\mathrm{c}_\vartheta}\right)\right\rvert T_{\mathrm{g}}$
$\|\Delta\hat{p}_{\mathrm{g}}\|$	$\lvert d_z\mathrm{s}_\varphi\rvert$	$\lvert d_x\left(1-\mathrm{c}_\vartheta\right) - d_z\mathrm{s}_\theta\rvert$

(12)

For easier interpretation, these results are also approximated by linearizing the most significant terms

	$\vartheta = 0$	$\varphi = 0$
$\|\Delta\hat{p}\|$	$\lvert v_y\varphi^2/2\rvert T_{\mathrm{g}}$	$\lvert v_x\vartheta^2/2\rvert T_{\mathrm{g}}$
$\lvert\Delta\hat{\psi}\rvert$	$\lvert\omega_y\varphi\rvert T_{\mathrm{g}}$	$\lvert\omega_z\vartheta^2/2\rvert T_{\mathrm{g}}$
$\|\Delta\hat{p}_{\mathrm{g}}\|$	$\lvert d_z\varphi\rvert$	$\lvert d_z\vartheta\rvert$

(13)

whose graphical evaluation is reported in Fig. 4, together with the corresponding data points extracted from the experimental dataset described in Section II. The analysis can be summarized as follows. With respect to the integration mismatch, captured by first and second metrics, the differences between the models in both position and yaw evolution remain limited under standard riding conditions. For $\vartheta = 0$, although the roll angle φ can reach significant values, the lateral speed v_y and the angular speed ω_y are usually small, with only few peaks occurring during slaloms or cornering. Conversely, when $\varphi = 0$, v_x and ω_z can be large, but the pitch angle ϑ stays within a narrow range. As a consequence, significant mismatches emerge only in extreme situations, such as high-roll drifts producing large v_y, or wheelie-like conditions combining high v_x with non-negligible ϑ. In addition, integration mismatches scale with the integration time T_{g}, making them more relevant at decreasing GNSS update rates. Nevertheless, as shown in Fig. 4, the position-related integration mismatches become comparable with the output equation mismatch only for $T_{\mathrm{g}} = 1$ s, i.e., when the GNSS operates at a very low update frequency. Conversely, the output equation mismatch is highly sensitive to variations in both roll and pitch. This comes from the fact that the vertical offset d_z between the GNSS antenna and the ground-projected CoG can be substantial, as the GNSS antenna must be mounted at elevated positions on the motorcycle to ensure unobstructed satellite visibility. As a result, even moderate roll or pitch angles induce noticeable deviations in the projected GNSS position, making the output mismatch significantly larger than the integration mismatch for typical riding conditions. This highlights that, in KF-based localization, neglecting roll or pitch primarily affects the correction step rather than the prediction step, with the magnitude of the induced error directly driven by the combination of φ, ϑ, and antenna height d_z.

IV. Experimental Analysis

In this section, after the derivation of the general analysis, the formal results regarding the influence of roll and pitch angles on the localization model are evaluated using the experimental dataset introduced in Section II for the target vehicle. The input to the localization models are obtained directly from the onboard sensors: roll/pitch angles together with linear velocities are retrieved from the OSU, while the angular rates are measured by the IMU. Reported analysis is just for the rear GNSS antenna position with respect to the CoG is $d_{\mathrm{g}} = \left[-825\ 0\ 1110\right]'$ mm, results for the front antenna are similar because both are placed at the same height. We analyze the modeling performance as a function of the GNSS output frequency f_{g}. Performance is quantified through two

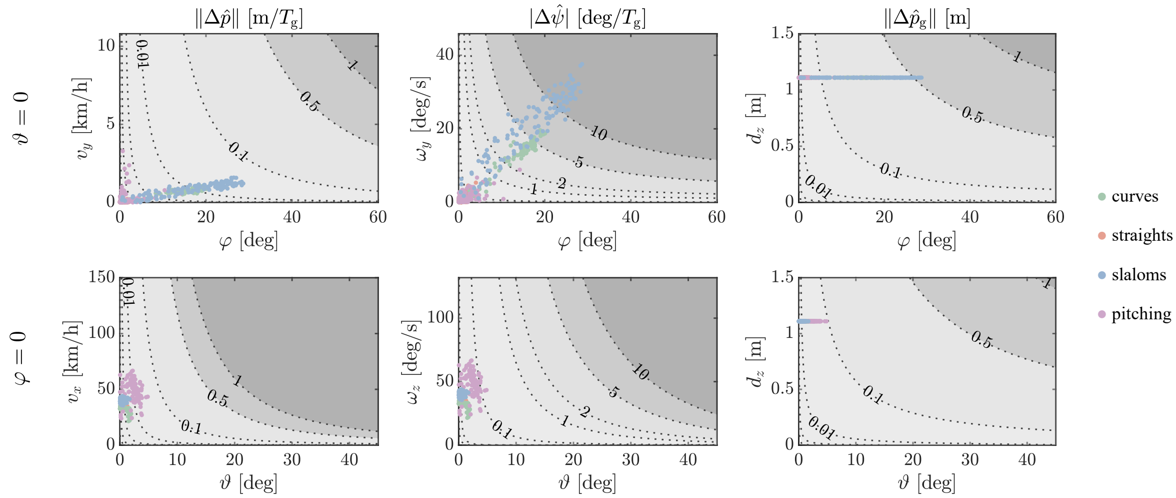

Fig. 4. **Localization Models Analysis**: mismatch metrics defined in (12), evaluated as function of roll and pitch angles. The plots also highlight the distribution of experimental data corresponding to the maneuvers classes introduced in Fig. 1.

indexes: the position integration error J_p, and the output error J_g, both computed with respect to a benchmark. The benchmark for the antenna position is obtained from the GNSS measurements p_g, as described in Section II. The benchmark CoG position p, instead, is reconstructed offline as

$$p = p_g - E \cdot R(\varphi, \vartheta, \psi_g) d_g, \tag{14}$$

which compensates for the known antenna offset through the measured vehicle attitude; indeed, ψ_g is the benchmark yaw angle obtained using information from the two available antennas. Therefore, the two indexes can be mathematically written in the discrete-time domain defined by the ECU running frequency f_0 as

$$J_p(k_0, f_g) = \frac{1}{1+\frac{f_0}{f_g}} \sum_{k=k_0}^{k_0+\frac{f_0}{f_g}} \|p - \hat{p}(k)\|, \tag{15}$$

$$J_g(k_0, f_g) = \frac{1}{1+\frac{f_0}{f_g}} \sum_{k=k_0}^{k_0+\frac{f_0}{f_g}} \|p_g(k) - \hat{p}_g(k)\|. \tag{16}$$

The quantities $\hat{p}$ and $\hat{p}_g$ are obtained through forward-Euler numerical integration of the localization models reported in Table I, using the benchmark values to initialize the integration window:

$$\hat{p}(k = k_0) = p(k_0) \text{ and } \hat{\psi}(k = k_0) = \psi_g(k_0). \tag{17}$$

The indexes are computed for every sample k_0 in the dataset, grouped according to the four selected maneuvers classes, as an average over a time interval determined by the chosen GNSS frequency f_g. The results of the analysis are illustrated in Fig. 5, where the two indexes are reported for each maneuver class as a function of the GNSS output frequency f_g. The f_g range is centered on 10 Hz, a typical value for current RTK-GNSS, and spans from 1 Hz to 100 Hz, i.e., from a low-cost commercial sensor to an ideal GPS sampling at the ECU frequency. For each frequency, the minimum, the maximum, and average values across all considered frequencies are shown. First, as expected from the analysis in Section III-B, the integration error J_p is similar across the models. Due to the limited influence of roll and pitch angles on the integration, these errors remain consistent across all tested maneuvers. Consequently, the primary factor affecting the integration error is the GNSS frequency, which determines the duration over which the model must propagate without correction. In contrast, significant differences are observed in the output error J_g by the height of the GNSS antenna, positioned over 1 m above the ground. Neglecting roll and pitch angles in the model leads to substantial errors in the predicted antenna position, with the largest discrepancies occurring during curves and pitching maneuvers, even at low GNSS frequency. These results are particularly relevant for KF-based localization algorithms. On the one hand, the correction step, that compares the predicted output against the measurements, can lead to incorrect state estimates if roll and pitch angles are neglected and the antenna is not mounted close to the ground. On the other hand, the effects of roll and pitch can be neglected in the prediction step.

V. Conclusions

In this paper, the impact of GNSS output frequency and antenna position in vehicle modeling for localization has been studied focusing on a motorcycle application. First of all, the impact of roll and pitch on the localization kinematic model has been mathematically approached. The experimental test are used to compare the localization model against RTK-GNSS measurements. Both the mathematical and the experimental analysis revealed that roll and pitch angles are fundamental to properly estimate the GNSS antenna position, which plays an important role in KF-based localization algorithms, since they affect the correction term; whereas the integration error is more sensitive to slower GNSS sampling frequency than roll and pitch values.

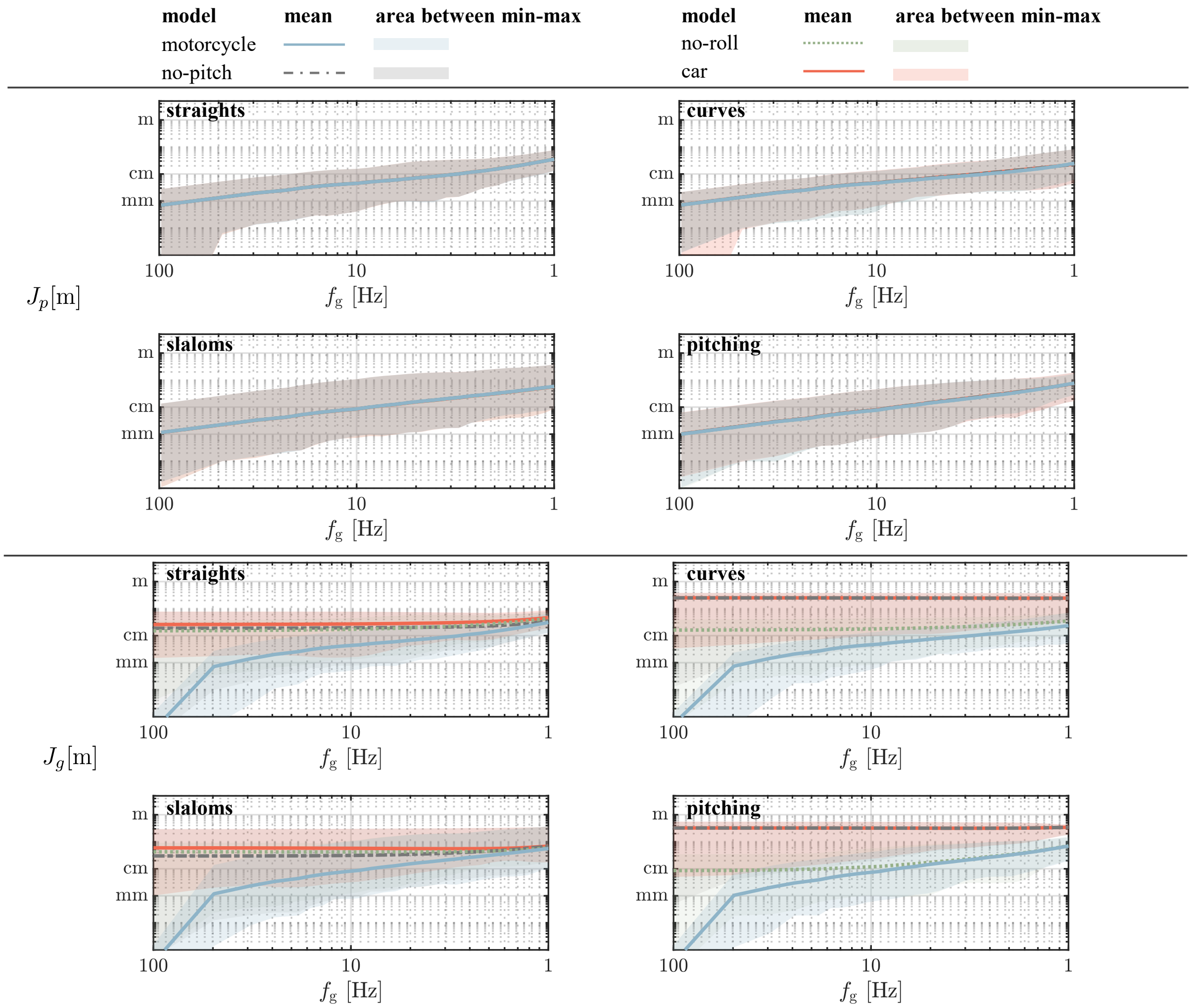

Fig. 5. **Experimental Analysis**: J_p (top) and J_g (bottom) indexes metrics, defined in (15) and (16), and their min-max area are evaluated as functions of GNSS output frequency for the different maneuvers classes introduced in Fig. 1.

Acknowledgments

The authors would like to thank Alberto Lucchini, Marcello Cellina, and Luca Varotto for their support.

References

[1] E. Yurtsever, J. Lambert, A. Carballo, and K. Takeda, "A survey of autonomous driving: Common practices and emerging technologies," *IEEE access*, vol. 8, pp. 58 443–58 469, 2020.

[2] Y. Zhang, J. Li, J. Yi, and D. Song, "Balance control and analysis of stationary riderless motorcycles," in *2011 IEEE International Conference on Robotics and Automation*. IEEE, 2011, pp. 3018–3023.

[3] K. Jo, J. Kim, D. Kim, C. Jang, and M. Sunwoo, "Development of autonomous car—part i: Distributed system architecture and development process," *IEEE Transactions on Industrial Electronics*, vol. 61, no. 12, pp. 7131–7140, 2014.

[4] D. Kumar and N. Muhammad, "A survey on localization for autonomous vehicles," *IEEE Access*, vol. 11, pp. 115 865–115 883, 2023.

[5] S. Specchia, A. Giacalone, R. Pieroni, G. Panzani, M. Corno, and S. M. Savaresi, "Autonomous vehicle localization on standard definition maps based on camera and lidar sensor fusion," in *2025 European Control Conference (ECC)*. IEEE, 2025, pp. 1395–1401.

[6] S. Gabrielli, G. Riva, L. Cattaneo, M. Corno, and S. M. Savaresi, "A fast lidar registration algorithm for autonomous racing: track constrained generalized iterative closest point (tc-gicp)," in *2025 European Control Conference (ECC)*. IEEE, 2025, pp. 1755–1760.

[7] Y. Liu, X. Fan, C. Lv, J. Wu, L. Li, and D. Ding, "An innovative information fusion method with adaptive kalman filter for integrated ins/gps navigation of autonomous vehicles," *Mechanical systems and signal processing*, vol. 100, pp. 605–616, 2018.

[8] G. Hu, S. Gao, and Y. Zhong, "A derivative ukf for tightly coupled ins/gps integrated navigation," *ISA transactions*, vol. 56, pp. 135–144, 2015.

[9] R. Song and Y. Fang, "Vehicle state estimation for ins/gps aided by sensors fusion and sckf-based algorithm," *Mechanical Systems and Signal Processing*, vol. 150, p. 107315, 2021.

[10] J. E. Espinosa, S. A. Velastín, and J. W. Branch, "Detection of motorcycles in urban traffic using video analysis: A review," *IEEE Transactions on Intelligent Transportation Systems*, vol. 22, no. 10, pp. 6115–6130, 2020.

[11] C. Hebisch, D. Benz, A. Lemmer, and D. Abel, "Mobile app driven localization for motorcycles based on an adaptive unscented kalman filter," in *2022 IEEE 25th International Conference on Intelligent Transportation Systems (ITSC)*. IEEE, 2022, pp. 3831–3836.

[12] S. Smaiah, R. Sadoun, A. Elouardi, B. Larnaudie, S. Bouaziz, A. Boubezoul, B. Vincke, and S. Espié, "A practical approach for high precision reconstruction of a motorcycle trajectory using a low-cost multi-sensor system," *Sensors*, vol. 18, no. 7, p. 2282, 2018.

[13] S. Radrizzani, C. Dallapè, and G. Panzani, "Design and experimental validation of a filter-based allocation strategy for the longitudinal dynamics control in an autonomous motorcycle," *IFAC-PapersOnLine*, vol. 59, no. 5, pp. 157–162, 2025, 11th IFAC Symposium on Advances in Automotive Control AAC 2025.

[14] B. Siciliano and O. Khatib, *Springer handbook of robotics*. Springer, 2008.